Authors: Dave Hannes
Magnus Dahlberg
Thomas Svensson
Andreas Anderson

Research

2017:25

Evaluation of weld fatigue reduction in austenitic stainless steel pipe components

SSM perspective

Background
The performed investigation is a continuation of the work performed in SSM 2015:38 where fatigue tests were performed on pressurized *welded* austenitic stainless steel piping components. The specimens were subjected to a realistic variable amplitude loading with mainly reversed bending deformation and particular focus on high cycle fatigue. The previous fatigue results were quite dependent on the estimation of the stress concentration factor of the weld. Therefore, it was decided to continue this research by performing fatigue tests on pressurized *non-welded* austenitic stainless steel piping components.

Objective
The present study is aimed to investigate the margins of the ASME design curve for austenitic stainless steel, by performing fatigue experiments on a realistic non-welded austenitic stainless steel piping component and compare the results with the previous study where fatigue experiments on welded austenitic stainless steel piping components were performed. In this way, a more realistic analysis can be made of the fatigue strength reduction factor (FSRF).

Another objective has been to improve the knowledge on the *transferability* for a non-welded piping component subjected to variable amplitude loading by comparing with smooth specimen data obtained with constant amplitude fatigue testing.

Results
Extensive conservatism in the ASME approach to deal with transferability was confirmed. For the considered welded piping, the ASME design curve corresponded to a reduction in allowable number of cycles with a factor of at least 2.3. For the welded piping component, the fatigue strength reduction factor FSRF was estimated to 1.8 by comparing the results from the welded and unwelded pipe experiments.

The work has increased the understanding of the ASME margins and has improved the knowledge on fatigue in austenitic stainless steel components and the fundamental issue of transferability.

Need for further research
There is a need to further verify the results of this study by performing more fatigue experiments on larger and thicker piping components and using other welding configurations. Also, there is a need to further investigate the complex material behavior of austenitic stainless steel be in order to better describe the strains at the weld toe or strain concentration.

Project information
Contact person SSM: Björn Brickstad
Reference: SSM2016-564

Authors: Dave Hannes, Magnus Dahlberg [1], Thomas Svensson [2]. Andreas Anderson [3]

[1] Inspecta Technology AB, Stockholm, Sweden
[2] TS Ingenjörsstatistik, Borås, Sweden
[3] RISE Research Institutes of Sweden, Borås, Sweden

2017:25

Evaluation of weld fatigue reduction in austenitic stainless steel pipe components

This report concerns a study which has been conducted for the
Swedish Radiation Safety Authority, SSM. The conclusions and view-
points presented in the report are those of the author/authors and
do not necessarily coincide with those of the SSM.

Evaluation of weld fatigue reduction in austenitic stainless steel pipe components

Summary

The performed investigation is a continuation of the work performed in SSM 2015:38 and consists of fatigue tests on water pressurized non-welded austenitic stainless steel piping components. The specimens are subjected to a realistic variable amplitude loading with mainly reversed bending deformation and particular focus on HCF.

The experimental results allowed to determine a weld fatigue strength reduction factor (FSRF) for a similar piping component with circumferential butt weld in as-welded condition from SSM 2015:38. It was estimated to about 1.8. Both Basquin and Langer fatigue models were used and yielded consistent results. The weld FSRF did not exhibit any dependency on load level or number of load cycles and could thus be assumed to be constant. The experimental estimate of the FSRF highlighted the conservatism of the ASME approach based on stress indices.

The resulting margins in the fatigue design curve for austenitic stainless steel in ASME III were investigated. Extensive conservatism in the ASME approach to deal with transferability was confirmed. For the considered welded piping, the ASME design curve corresponded to a reduction in allowable number of cycles with a factor of at least 2.3. For the non-welded piping component, the fatigue life reduction factor was minimum 1.6. The ASME design curve represents thus a survival probability largely in excess of 95 % for the considered realistic components and loading configurations.

The experimental investigation resulted in increased understanding of the effect on the fatigue strength for piping components of a welding joint in as-welded condition. It improved the knowledge on the crucial issue of transferability and increased fundamental understanding for fatigue in piping components.

Contents

1 Nomenclature

A	Factor in Langer equation
B	Exponent in Langer equation
C	Cut-off or asymptotic limit in Langer equation
E	Young's modulus
i	Dummy index
k	Scaling factor for strain amplitudes
K_f	Fatigue strength reduction factor
K_t	Concentration or notch factor
m	Total number of strain cycles in a load sequence
n	Total number of strain cycles in a load sequence with amplitudes exceeding the cut-off limit
N	Total number of cycles, predicted or experimental fatigue life
N_C	Total number of load cycles with strain amplitudes exceeding the cut-off limit C
q	Notch sensitivity factor
R_m	Tensile strength
$R_{p0.2}$	Yield strength
t	Nominal wall thickness
α	Factor in Basquin equation
β	Exponent in Basquin equation
ε	Strain (axial)
ε_0	Mean nominal strain (due to internal pressure)
ε_a	Strain amplitude
ε_m	Mean strain
σ	Standard deviation of error of predicted logarithmic life
$\hat{\blacksquare}$	Estimated quantity
$\blacksquare_{max}$	Maximum value
$\Delta\blacksquare$	Range or change

2 Introduction

2.1 Background

Rules for construction or design of nuclear facility components are specified in section III of the ASME Boiler and Pressure Vessel Code [1]. The design against fatigue is based on the use of prescribed material specific fatigue design curves (Wöhler diagrams). Such design curves correspond to at least 95% survival probability and are derived by adjustment of a mean curve. The mean curve is typically obtained by fitting to relatively large amounts of data from mainly laboratory experiments in air on small, smooth test specimens subjected to constant amplitude loading. The fatigue design curves are however intended for real components subjected to realistic loading. The adjustment of a mean curve therefore needs to account for the fundamental and challenging issue of transferability. It is essential in understanding and preventing fatigue in real or relevant components, but is affected by a large amount of variables [2]. The fatigue design curves in ASME III [1] are obtained by correcting the mean curve with adjustment factors on the strain (or stress) or the cycles, whichever is more conservative. The fatigue design curve in ASME III [1] for austenitic stainless steel (SS) is obtained from an adjustment of a mean curve derived by ANL [2]. The adjustment factor for strain (or stress) is equal to 2 and the one for the number of cycles equals 12. Prior to 2010, the latter adjustment factor equaled 20 and a revised version of [2] including new experimental data proposes to reduce the adjustment factor on the number of cycles to 10. The conservatism or margins of the fatigue design curves in ASME III [1] is thus closely related to the magnitude of these adjustment factors.

The fatigue design curves in ASME III [1] are to be used in conjunction with a local fictitious (elastic) stress amplitude. The local stress measure can be determined from a nominal stress and different stress indices defined in ASME III [1], which account for various effects related to geometry or loading. The stress concentration, i.e. when the local stress exceeds the nominal stress, will typically result in a local fatigue strength reduction of the component or structure. Following the definition in NB-3200 of ASME III [1], the fatigue strength reduction factor (FSRF) is a stress intensification factor which accounts for the effect of a local structural discontinuity (stress concentration) on the fatigue strength. Applying this definition to a welding joint yields that the FSRF for a given weld, material, component geometry and loading configuration is given by the ratio of the non-welded component's fatigue strength and the fatigue strength of the same component with the considered welding joint. The assessment is performed for a given number of cycles. The FSRF is typically determined through experiments, but in the absence of experimental results the FSRF is often approximated by the stress concentration factor, i.e. the ratio of a local and a nominal stress measure. The latter being defined such that any effects of the local structural discontinuity are excluded, i.e. typically some distance away from the stress concentration. Welding joints typically represent a local structural discontinuity and the stress indices used in piping design specified in NB-3600 of [1] can be interpreted as a FSRF [3]. The FSRF increases with number of cycles and reaches a maximum value at the fatigue limit or high cycle fatigue (HCF) regime [3]. This maximum value is often used as a conservative design measure also applicable for low cycle fatigue (LCF). A reduction of the fatigue design curves with a FSRF allows their use in conjunction with a nominal stress measure.

2.2 Performed Piping Component Fatigue Tests

The margins of the fatigue design curve for austenitic stainless steel in ASME III [1] were subject to investigation in [4], where water pressurized welded stainless steel piping components were subjected to variable amplitude (VA) primarily reversed bending deformation, i.e. component testing or fatigue experiments under realistic conditions. The welded piping component and experimental set-up are illustrated in Figure 1. The nominal wall thickness in the central part of the test specimen, i.e. in the region including the circumferential butt weld, was 3 mm. The welding joint was in as-welded condition, i.e. the weld capping was not removed and induced a local stress concentration. Fatigue failure was defined by leakage, i.e. when the internal pressure of 70 bar could no longer be sustained. The experimental set-up was based on a construction using custom-built fixtures, which introduced a predominant bending stress and a small membrane stress. The work performed in [4] had particular focus on HCF and VA loading. The fatigue experiments included however both constant amplitude (CA) fatigue tests and experiments with VA loading using different load spectra, amongst which a synthetic Gaussian spectrum, designated with VAG. Additional information about the used test specimens, experimental set-up, testing procedure, load description and/or obtained results from the performed fatigue tests is available in [4, 5, 6, 7].

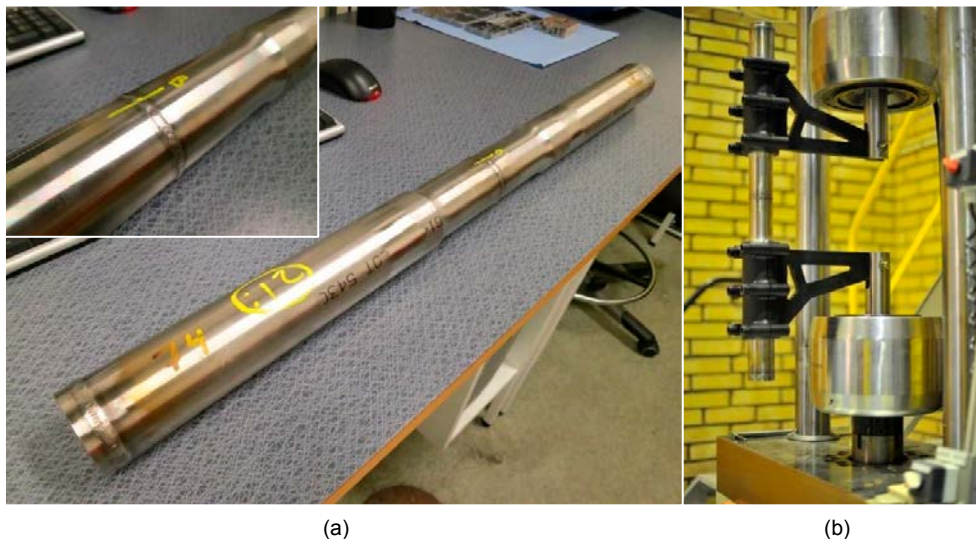(a)   (b)

Figure 1. (a) Welded piping component with close-up view of the circumferential butt weld in as-welded condition. (b) Actual mounted test specimen in servo-hydraulic testing machine with custom-built fixtures.

The performed work in [4] consisted of the determination of a component specific design curve derived from recorded nominal strain amplitudes. Comparison with the fatigue design curve in ASME III [1] allowed a better understanding of the margins in the ASME design curves and quantify the degree of conservatism. In the case of welded piping components, the presence of the welding joint induced a stress concentration. Hence the need to use a weld fatigue reduction factor to allow for the ASME fatigue design curve to be used in conjunction with nominal strain amplitudes. The work in [4] considered both a FSRF of 3.24 based on stress indices defined in NB-3600 of ASME III [1] and a FSRF approximated by a stress concentration factor of 1.4 computed by a finite element (FE) analysis. The findings in [4] highlighted extensive conservatism, but the extent of the margins in ASME was shown to largely depend on the weld fatigue reduction factor used.

2.3 Objectives

The current investigation is a continuation of the work performed in [4] and consists of fatigue tests on pressurized non-welded austenitic stainless steel piping components, with realistic VA loading and with particular focus on HCF. The empirical approach with a synthetic spectrum load developed in [4] will be applied. Through comparison with the results for the welded piping component in [4], a weld FSRF will be determined. The study will thus provide a revised and verified value for the weld fatigue reduction factor in [4]. The resulting margins in the fatigue design curve for austenitic stainless steel in ASME III [1] will be assessed by revising the findings from [4].

The work aims at

- increasing understanding of the effect of a welding joint on fatigue life for piping components by improving the knowledge about the difference in fatigue strength between non-welded and welded pipes.

- facilitating future discussions about margins and conservatism in ASME III [1].

- improving the knowledge on transferability for a non-welded piping component subjected to variable amplitude loading by comparing with smooth specimen data obtained with constant amplitude fatigue testing, see [2].

- further increasing insight in how to efficiently handle and mitigate potential fatigue risks in austenitic stainless steel components, i.e. increase fundamental understanding for fatigue in piping components.

3 Experimental study

The results in the current investigation were obtained with a limited number of test specimens and realistic testing conditions.

3.1 Test specimens

A total of 19 test specimens were manufactured from straight, seamless TP 304 L stainless steel hot finished pipes. All specimens were manufactured from the same batch: lot 50260. Table 1 contains the chemical composition and Table 2 presents the tensile properties at room temperature of the material. The material was thus similar to the one used in [4], but the manufacturing process of the pipes did differ. The current pipes were hot worked (extruded), whereas the pipes in [4] were cold worked (rolling). The effect of this difference in manufacturing process on the fatigue material behavior of the test specimens was considered to be small.

Table 1. Chemical composition as percentage by weight [weight%] for lot 50260.

C	Si	Mn	P	S	Cr	Ni	Mo	Co	Cu	N
0.016	0.38	1.21	0.029	0.008	18.20	10.13	0.34	0.11	0.32	0.051

Table 2. Average tensile properties at room temperature for lot 50260.

Yield strength $R_{p0.2}$ [MPa]	Tensile strength R_m [MPa]	Elongation [%]	Young's modulus E [GPa] (*)	Poisson's ratio [-]
240	600	60	200	0.3

(*) Sandvik 3R12

The original pipe geometry was identical to the one used in [4]: the pipe nominal outer diameter was 60.33 mm with a nominal wall thickness equal to 5.54 mm. The pipes were partially machined to introduce shoulders by reducing the outer diameter until a remaining wall thickness of approximately 4 mm. This first diameter reduction was introduced to reduce the risk for failure due to contact fatigue (fretting) under the fixtures. In order to further reduce the volume of material subjected to significant fatigue loads and localize fatigue failure, an additional diameter reduction was introduced in the center of the specimen. More specifically a circumferential notch with a fairly large notch radius of 75 mm was machined resulting in a nominal wall thickness of 3 mm in the symmetry plane of the test specimen. Figure 2 presents the geometry of the notched test specimens in more detail.

The internal surface roughness of the test specimens was somewhat greater in the current study than for the welded piping components used in [4]. However failure is expected to occur in the notch, i.e. on the external machined surface presenting a finer surface roughness. The increased surface roughness on the inside of the specimens is thus not expected to affect the fatigue behavior.

After machining of the test specimens, see Figure 3, the pipes were fitted with approximately 7 mm thick butt welded lids to allow pressurizing during the experiments. The lids were equipped with a fitting to allow control of the internal pressure.
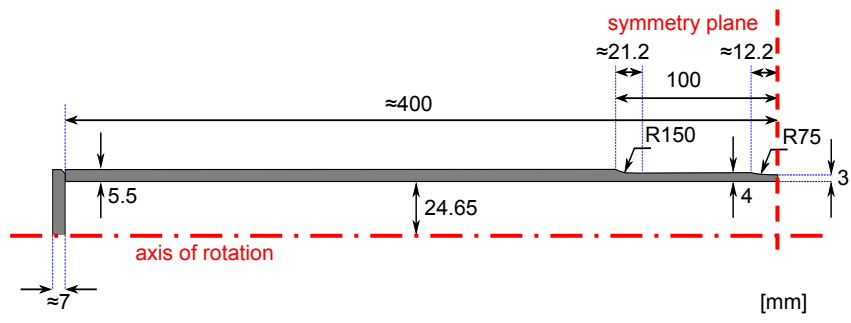
Figure 2. Schematic of the geometry of the piping component.

Figure 3. Different test specimens after machining and prior to welding the lids at the extremities.

3.2   Experimental set-up

3.2.1   Equipment and instrumentation

The experimental set-up consisted of the same custom-build construction as used in [4] allowing for reversed bending loading with displacement control in a standard single axis servo-hydraulic testing machine, see Figure 4. The distance between the grips was approximately 205 mm. Nominal (elastic) strains are linearly related to applied displacement, which supports the use of displacement control in the performed fatigue experiments [4]. Conventional strain gages were mounted on the test specimen in the axial direction at positions A and B, see Figure 4(b). The gage length was relatively short, 2 mm, allowing to get more accurate estimates of local peak values. Fatigue crack initiation was reported to occur in the vicinity of these locations for the experiments with welded piping components in [4]. These two positions are situated in the symmetry plane of the specimen, i.e. in the notch, and in the bending plane, i.e. the plane with the largest bending stresses. Position A is situated closest to the testing machine, where bending and membrane stresses act in phase, inducing maximum strain amplitudes. At position B the maximum bending stresses are in opposite phase from the membrane stresses resulting in somewhat lower maximum strain amplitudes [6]. The local axial strains in the notch were thus recorded during testing, as opposed to the nominal strain measure recorded in [4]. During the pre-testing phase of the experimental series some tests were however performed where also nominal axial strains were recorded similarly as in [4], i.e. approximately 50 mm from the notch.
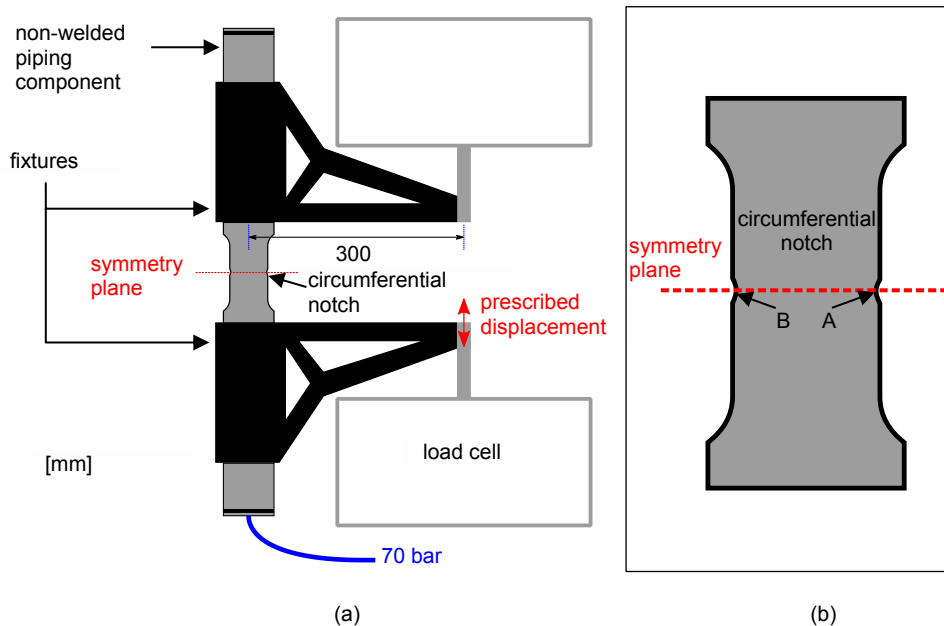

Figure 4. (a) Schematic of experimental set-up for alternating bending fatigue testing. (b) Schematic close-up view of the machined part of the specimen with the circumferential notch and strain gage positions A and B.

3.2.2 Testing procedure

The fatigue experiments were displacement controlled with load ratio approximately equal to minus unity. Displacement control allows for realistic and relevant load definition. During the course of the fatigue experiments the resulting force in the load cell and the local axial strain measures at A and B for the test specimen were recorded with a sampling frequency of 200 Hz. The tests were performed in air at room temperature (RT), avoiding environmental effects on the fatigue behavior of the piping component, which was out of the scope of the current investigation. The piping components were furthermore water pressurized allowing for a realistic failure criterion based on leakage. The experiments were stopped when leakage was detected by the pressure actuator displacement increase to a pre-set level. Alternatively fatigue experiments were stopped when a run-out limit of 11000 load blocks (corresponding to approximately 5 million cycles) was reached or exceeded.

3.3   Load description

The 19 piping components included in the experimental test series were mainly subjected to a synthetic Gaussian variable amplitude loading, which was scaled to 10 different severities, see Table 3. The bending deformation together with the internal pressure introduced a relevant multi-axial load state, as for the experiments in [4]. The constant internal pressure was 70 bar and yielded a tensile mean strain in the axial direction. The nominal axial strain contribution of the internal pressure was estimated to approximately $\varepsilon_0 = 0.0040$ %, based on linear elastic material behavior. This mean strain was considered small compared to the applied maximum strain amplitudes. Although increased test frequencies are convenient to reduce the total testing time, the testing frequency in the accelerated fatigue experiments was limited to avoid too large strain rates. No strain rate effects on the fatigue behavior were expected during the fatigue experiments at RT [2]. In the current investigations strain rates did usually not exceed 10%/s, except for cycles with large amplitudes in experiments with displacement amplitudes larger or equal to 4 mm.

Table 3. Summary of different load types considered in the fatigue experiments.

Load type	Total number of tests	Number of tested severities
Constant amplitude (CA)	2	2
Gaussian variable amplitude (VAG)	17	10

3.3.1   Constant amplitude (CA)

The two constant amplitude experiments were performed with sinusoidal prescribed displacement signals. The severity of the prescribed displacement was determined by its amplitude: 1.95 or 3.1 mm. The corresponding local strain amplitudes in A were 0.17 and 0.23%, respectively.

3.3.2   Gaussian variable amplitude (VAG)

A Gaussian spectrum similar as the one used in [4] with 453 cycles per load block was used. A load block lasted 43.2 s and consecutive load blocks were separated by a brief transition or hold time. The hold time was in the range 0.5 - 1 s. A normalized load block is illustrated in Figure 5. The normalized axial strain signal was obtained by subtracting mean strain and dividing by the maximum strain amplitude. Ten severity levels were examined by scaling up the magnitude of the prescribed displacement. The recorded local maximum strain amplitude in A were in the range 0.2 – 0.4%, hence always exceeding the yield strain of 0.12%.
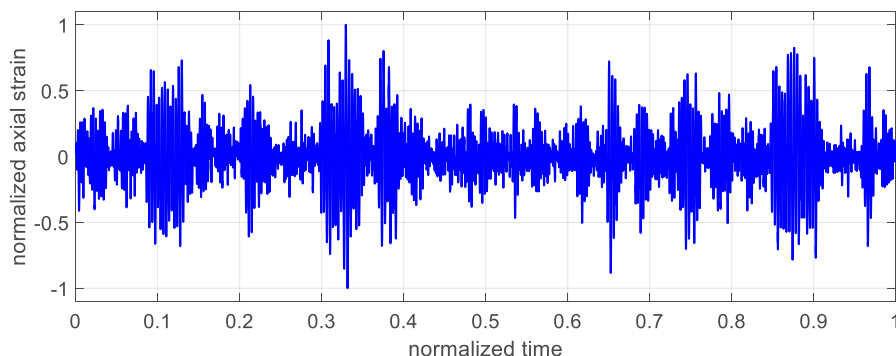

Figure 5. Normalized recorded strain signal in A corresponding to a load block of the VAG spectrum.

4 Theory and methods

4.1 Fatigue life models

Different models exist to predict the number of cycles to component failure as function of a load parameter, such as stress or strain amplitude. In the current experimental investigation the selected fatigue governing parameter was the measured strain amplitude, which allowed direct comparison with ASME predictions and further study of the ASME margins in the continuation of the work performed in [4].

The experimental results from the performed alternating fatigue bending tests on piping components were investigated with two different models with a scalar strain amplitude load parameter. The original models were generalized to be applicable with variable amplitude loading. A norm or equivalent strain amplitude was therefore introduced based on Palmgren-Miner's linear damage rule [8, 9]. This hypothesis is in accordance with the ASME procedure. The methodology of this procedure is further detailed in [10] and is identical to the one applied in the previous work [4].

4.1.1 Basquin model

Basquin's equation without a fatigue limit is a classic approach to model high cycle, low strain amplitude fatigue. A linear relation in logarithmic form is assumed, between the strain amplitude and the total number of load cycles, N [11]. In the current investigation with variable amplitude loading an equivalent strain amplitude $\|\varepsilon_a\|_\beta$ is used,

$$N = \alpha \left(\|\varepsilon_a\|_\beta \right)^{-\beta} \tag{1}$$

The constants α and β are typically determined by fitting to experimental data. The equivalent strain amplitude gives the same accumulated damage as the full spectrum and is defined as the β-norm of the strain amplitudes $\varepsilon_{a,i}$ included in a load sequence consisting of m strain cycles,

$$\|\varepsilon_a\|_\beta = \left(\frac{1}{m} \sum_i^m \varepsilon_{a,i}^\beta \right)^{1/\beta} \tag{2}$$

4.1.2 Langer model

The Langer model [12] uses a modified expression of the Basquin relation in Equation (1) including a cut-off limit introducing a characteristic curved shape for long lives. The design curves in the ASME standard [1] are based on fittings presented in [2] using the Langer model. The Langer equation is expressed in terms of constants A and B, analogues to α and β in Equation (1), and an additional constant C introducing an asymptote in the model. For variable amplitude loading the equivalent strain amplitude $\|\varepsilon_a\|_{BC}$ is introduced,

$$N = A \, (\, \|\varepsilon_a\|_{BC} - C \,)^{-B} \tag{3}$$

The equivalent BC-norm of the strain amplitude gives the same accumulated damage as the full spectrum and is expressed, by analogy with Equation (2), in terms of constants B and C.

$$\|\varepsilon_a\|_{BC} = \left(\frac{1}{n} \sum_i^n (\varepsilon_{a,i} - C)^B \right)^{1/B} + C \tag{4}$$

The sum only includes the n cycles for which the strain amplitudes exceed the threshold level C. Note that for $C = 0$, the Basquin relation from Equation (1) is recovered, i.e. all strain cycles of the considered load sequence contribute to fatigue damage accumulation.

4.1.3 Maximum-likelihood methodology

The maximum-likelihood methodology is a general method for fitting model parameters to empirical models. It is a probabilistic approach that as inputs needs,

i. a model formulation with parameters to be fit,

ii. a number of empirical observations of a property,

iii. an assumption of a random distribution type for the observed property.

In case of the two considered fatigue models the observed property is fatigue life and the two model formulations, Basquin and Langer have two and three fitting parameters, respectively. For each model, it is assumed that the logarithm of life follows a normal distribution with the expected value according to the model and an unknown standard deviation. The procedure used in the current investigation for determination of the model parameters is identical to the one applied in [4]. More details on the methodology are found in [10].

4.2 Transferability

The ANL mean curve from [2] was derived from fatigue tests on small, smooth test specimens. The current study performed however fatigue tests on a realistic smooth component. The expected difference in fatigue strength will illustrate the fundamental issue of transferability, i.e. the transfer from smooth test specimen results to predictions for real components. The former typically having a larger fatigue strength. In applications the fatigue strength of welded piping components is often limiting, as the welding joint introduces a stress concentration. The presence of a weld will result in a fatigue strength reduction of the component. The extent of this reduction can be quantified knowing the SN curve of the smooth component without a weld. The obtained SN curves from the current investigation correspond to those for the smooth piping component. Through comparison with the results for the welded piping component in [4], the amount of fatigue strength reduction can be determined.

4.2.1 FSRF estimation

The FSRF or the fatigue strength reduction factor is related to the fatigue strength measured as strain amplitude. The strain amplitude for the welded component should thus be multiplied with the FSRF to predict life using any of the plain piping fatigue models, Basquin or Langer.

By assuming that a constant FSRF fully describes the difference between plain and welded experimental results, K_f can be estimated from the recorded data. The numerical procedure is based on a multiplication of the nominal weld strain amplitudes included in the applied Gaussian and piping spectra from [4]. The optimal factor being an estimate of K_f is then determined by the maximum-likelihood procedure applied to both sets of experimental results, i.e. plain and welded. The considered fatigue model is thus fitted simultaneously to the valid VA data from the current study for non-welded specimens and scaled VA data from [4] for the welded pipes.

For the Basquin case, the model used in the likelihood estimation reads,

$$\ln N = \ln\alpha - \beta \ln\left(\|k\,\varepsilon_a\|_\beta\right) = \ln\alpha - \beta \ln\left(k\|\varepsilon_a\|_\beta\right) \qquad (5)$$

Similarly, for the Langer case the model is given by,

$$\ln N = \ln A - B \ln\left(\|k\,\varepsilon_a\|_{BC} - C\right) \qquad (6)$$

In these model formulations the scaling factor $k = 1$ for plain specimens and a positive constant for the welded piping components.

The possibility of a FSRF varying with amplitude was also considered. In the case of the Basquin model, such a variation would result in different slopes for welded and non-welded specimens when their parameters are estimated independently. The difference in slopes was a posteriori found not significant, which motivates the simple constant FSRF model used, see experimental results.

4.2.2 Determination of ASME margins

The margins of the ASME design curve are determined or quantified through comparison with component specific design curves derived with the empirical approach detailed in [4]. The parameter fitting with the maximum likelihood methodology results in an estimate of the standard deviation of logarithmic life. This estimate allows an approximate determination of the lower 90% prediction limit, which corresponds to a design curve for 95% survival probability. This design curve is component specific and can be compared to the corresponding design curve prescribed by ASME.

In the case of the current study the component specific design curve is derived with local strain amplitude measures, and can therefore be directly compared to the ASME design curve, which is intended for use in conjunction with local strain measures. In the case of the previous work with welded piping components [4], the recorded strain was the nominal strain. Hence the component specific design curve derived for the welded piping component is to be compared with a reduced ASME design curve, in order to get an estimate of its margins. The reduction of the ASME design curve was in [4] performed with different numerical estimates of the FSRF yielding relative uncertainty about the extent of the margins. In the current study however, the reduction is performed with an experimental estimate of the FSRF.

5 Results

5.1 Preliminary investigation

5.1.1 Notch effect

The CA test of pipe 02 was apart from strain recordings for the local strains in the notch also equipped for nominal strain readings with an additional strain gage positioned about 50 mm from the notch, i.e. similar as in [4]. The start of the experiment included a short sequence with low strain amplitudes ensuring fully elastic material behavior even in the notch. Comparison between the local strain in the notch and the nominal strain resulted in an estimated (elastic) notch factor $K_{t|t=4\ mm} = 1.6$. This notch factor designates the elastic strain concentration in the notch to the nominal strain recorded for a wall thickness equal to 4 mm. The welded piping component in [4] did however have a wall thickness of 3 mm. Through conservation of internal bending moment, the ratio of elastic nominal strains can be approximated by the inverse of the ratio of the nominal wall thicknesses. Hence, $K_{t|t=3\ mm} \approx 0.75\ K_{t|t=4\ mm}$, which yields an updated (elastic) notch factor $K_{t|t=3\ mm} = 1.2$. The strain in the notch of the investigated piping component is thus about 20% larger than the expected nominal strain for the corresponding un-notched piping component with wall thickness 3 mm.

The fatigue strength reduction factor K_f is defined as the ratio of the fatigue strength for the un-notched specimen and the fatigue strength for the notched specimen. The fatigue strengths considered are taken for a given number of cycles. Different numerical or analytical methods to estimate the fatigue strength reduction factor K_f accounting for the presence of the notch exist [13, 14]. A classic approach is to relate the FSRF to the notch or elastic stress/strain concentration factor K_t by means of the notch sensitivity factor q varying between 0 and 1,

$$K_f = 1 + q(K_t - 1) \tag{7}$$

For $q = 0$, the material is considered to be notch insensitive and $K_f = 1$, i.e. that the presence of a notch does not affect the fatigue strength, as plastic deformation in the notch effectively reduces the stress concentration. However for $q = 1$ or large notch sensitivity of the material, the FSRF is considered equal to the notch factor, i.e. $K_f = K_t$. In this case no redistribution of stress through local plasticity is expected. For common steels the notch sensitivity is expected to be close to unity given the large notch radius equal to 75 mm. However austenitic steels are known to present good notched fatigue strength, and thus a relatively low notch sensitivity [15]. Handbook recommendations [16] consider for annealed austenitic stainless steel that q is in the range 0.2 – 0.4 and increases with K_t. For the current application the notch factor is fairly low, hence a notch sensitivity of 0.3 can be considered as a conservative estimate. Consequently the FSRF for the notched smooth piping component compared to a smooth un-notched piping component with wall thickness 3 mm is equal to $K_f = 1 + 0.3\ (1.2-1) = 1.06$, which is very close to unity.

The notch was introduced to localize fatigue failure and reduce the volume of tested material. It will inevitably induce a reduction of the components fatigue strength compared to the un-notched specimen. For the current test series however the reduction is considered negligible. As a result, the smooth piping component with a large machined notch used in the current study has a fatigue strength similar to the un-notched smooth piping component with wall thickness 3 mm. This is an important result as knowledge about the reference fatigue strength curve for the un-notched smooth piping component is crucial in the experimental determination of the FSRF for the welded piping component in [4].

5.1.2 Inelastic material behavior

Inelastic deformations at relatively low loads are reported for austenitic stainless steel in [17]. During fatigue testing of the welded piping components in [4], the nominal strain recordings also indicated non-linear material behavior. In the current investigation similar non-linear material behavior was therefore expected and indeed observed. The observation of non-linear material behavior was even more pronounced as, contrary to the previous study, the local strain in the notch was recorded. Load spectra did indeed always include a certain amount of load cycles inducing strain amplitudes exceeding the material's yield strain. As a result, plastic deformations were rapidly induced in the vicinity of the locations A and B in the notch.
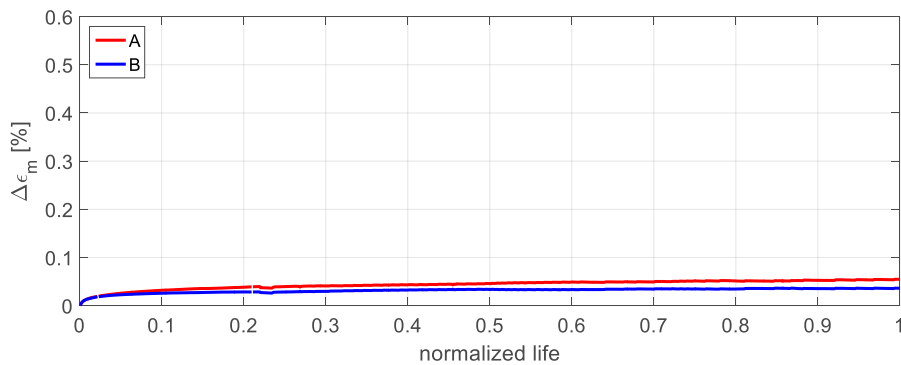
(a)   Results for pipe 8.
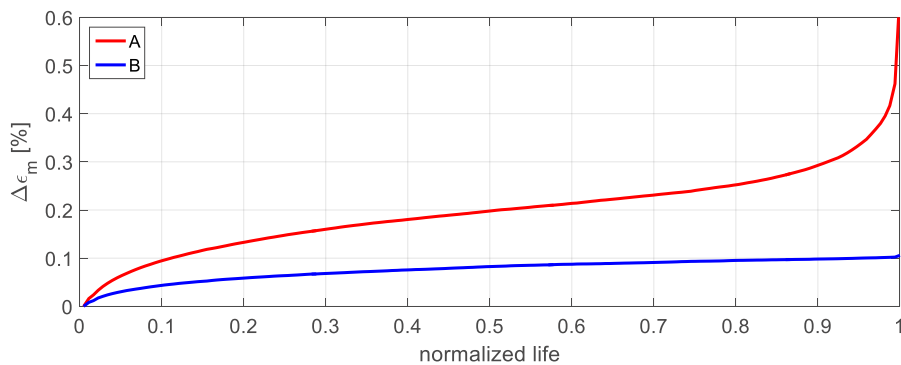
(b)   Results for pipe 14.

Figure 6. Illustration of the recorded increase in local axial mean strain ($\Delta\varepsilon_m$) in both A and B locations during fatigue testing for two different severities: (a) a low and (b) a relatively high fatigue load.

The internal pressure is a primary load and introduces a tensile axial mean strain. It was however observed that the axial mean strain increased during fatigue testing, especially in the case of significant cyclic loading. A cyclic secondary load, introduced through prescribed displacement, consists of reversed bending and membrane loads. The austenitic stainless steel piping component subjected to this load combination exhibited ratchetting behavior, i.e. progressive accumulation of inelastic strain. The accumulation of inelastic strain did have little effect on the recorded strain amplitude used in the fatigue assessment, but affected considerably the mean axial strain. Figure 6 illustrates, for a selection of two tests, the increase in axial mean strain recorded in the notch as function of the normalized testing time or fatigue life. The increase in location A always exceeded the one recorded in B. The difference in ratchetting behavior between A and B is explained by the difference in cyclic deformation at these locations. For relatively low cyclic loading, see Figure 6 (a), the progressive accumulation of inelastic axial strain occurs primarily during the early stages of the test. After this initial period the accumulation or increase in axial mean strain is relatively small or negligible. However for increased cyclic loading, see Figure 6 (b), significant accumulation of inelastic axial strain continued during the entire experiment.

5.2 Experimental fatigue results

A total of 19 fatigue experiments were performed during the current study. Only 13 experiments were however considered valid for performing the projected investigation. The results of these experiments are reported in Table 4 and Figure 7. The piping components were water pressurized which allowed for the failure criterion based on leakage. The presence of water drops in the circumferential notch was an illustration of ongoing leakage, see Figure 8, and indicating the presence of a penetrating fatigue crack. Only one experiment (pipe 8) was terminated prior to leakage detection, as the run-out limit of 11000 load blocks was reached. The total number of strain cycles to which each tested piping component was subjected is denoted N, including thus also strain cycles with small strain amplitudes contained in the VAG load spectra. The different equivalent strain measures were computed once the model parameters were estimated, see Section 5.2.2, from the local axial strain recordings in location A. All valid fatigue tests presented leakage in the vicinity of A, where the strain amplitudes were in average about 15% higher than those recorded in B. Locations A and B are defined in Figure 4.

The total number of strain cycles actually causing fatigue damage according to the Langer model is given by N_C. This quantity was computed by only considering the strain cycles to failure with amplitudes exceeding the threshold C. The BC-norm strain and N_C are directly related. $N_C < N$ for the data points which yields a shift leftwards in Figure 7, when only the number of cycles actually causing fatigue damage would be considered instead of the total number of cycles to failure.

Table 4. Experimental results from valid VAG fatigue tests. The β-norm was computed with β= 4.0 and the BC-norm with B = 2.07 and C= 0.056%. The strain measures are all based on the recorded local strain in location A.

Pipe ID	Severity[*]	N [cycles]	max ε_a [%]	$\|\varepsilon_a\|_\beta$ [%]	$\|\varepsilon_a\|_{BC}$ [%]	N_C [cycles]
4	4	608832	0.35	0.123	0.109	240119
6	3.7	1270665	0.25	0.093	0.091	421851
(†)8	3	4983000	0.23	0.084	0.085	1400843
9	3.3	1630347	0.28	0.101	0.095	537982
10	3.05	4061145	0.23	0.085	0.086	1139689
11	4.3	343374	0.39	0.140	0.121	158269
12	4.3	363759	0.41	0.141	0.120	158599
13	3.05	4449819	0.21	0.082	0.084	1364373
14	4	719364	0.33	0.117	0.105	289784
15	4.5	490146	0.39	0.139	0.120	219483
16	3.4	1474968	0.21	0.082	0.084	450191
17	3.2	3093084	0.22	0.080	0.082	822439
19	4.5	416760	0.38	0.137	0.118	189513

[*] The severity corresponds approximately to the maximum prescribed displacement amplitude in mm.
(†) Run-out experiment, where the number of cycles exceeded the run-out limit of 11000 load blocks.
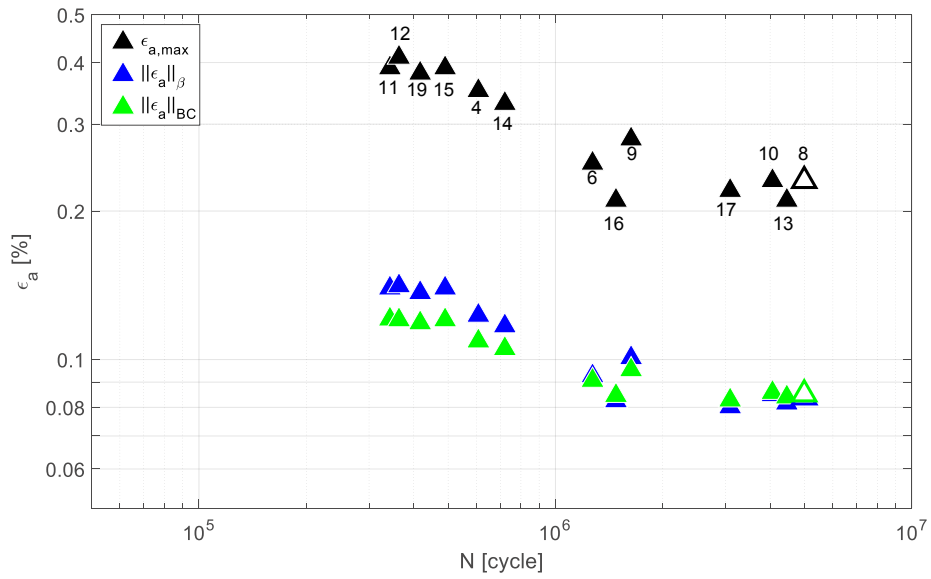
Figure 7. Experimental results with different strain measures for the 13 valid fatigue experiments on smooth piping components. The empty marker indicates a run-out and the numbers next to the black markers correspond to the pipe ID.
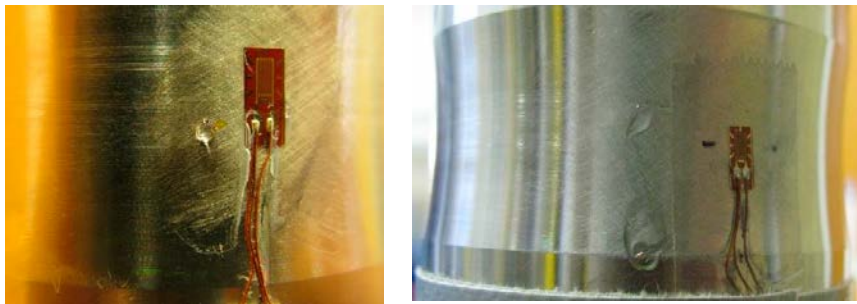

Figure 8. Axial strain gage mounted in the circumferential notch and water drops indicating leakage.
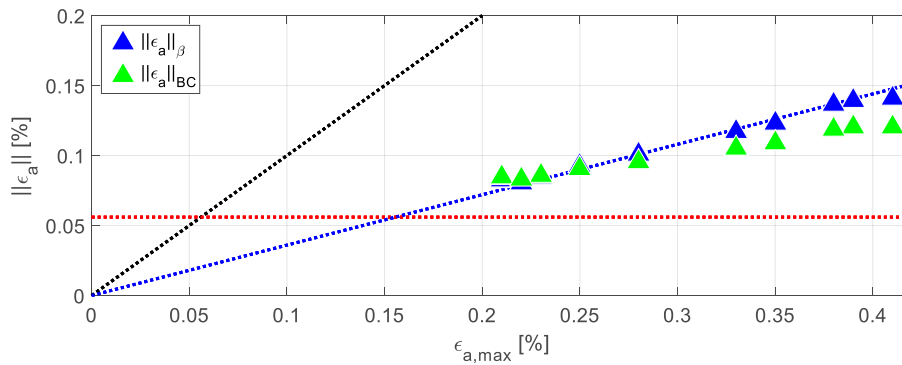

Figure 9. Relation between equivalent strain measures and maximum strain amplitude in the VAG spectrum. The β-norm was computed with $\beta = 4.0$ and the BC-norm with $B = 2.07$ and $C = 0.056\%$.

Contrary to the maximum strain amplitude, the equivalent strain measures account for the presence of lower strain amplitudes included in the load sequence. Hence the considerably lower values presented for the fatigue results with the VAG spectrum in Figure 7. Considering that even lower strain amplitudes will contribute to fatigue damage accumulation, the maximum strain amplitude will represent an over-estimation of the effective load. The equivalent strain measures are therefore more appropriate as fatigue parameters for VA loading. Figure 9 illustrates in more detail the relation between the equivalent strain measures and the local maximum strain amplitude. CA data points would be situated on the first bissectrice represented by the black dotted line. VA data points are however expected to be situated below the first bissectrice.

For a given spectrum, a proportional relation exists between the β-norm and the maximum strain amplitude of the considered spectrum. The constant of proportionality is, for a given spectrum, solely dependent on the value of β. For the current study considering the VAG spectrum with $\beta = 4.0$, the constant of proportionality is about 0.36, which is illustrated graphically by the blue dotted line in Figure 9. The β-norm in the current study is indeed about 36% of the maximum strain amplitude. More generally, for any spectrum the ratio of proportionality increases with β and tends to 1 for large values of β. For β tending to infinity, the infinity norm or maximum norm is indeed recovered, which then equals the maximum strain amplitude of the spectrum. In the case of the BC-norm, no proportional relation can be defined due to the effect of the cut-off limit C in the definition of the norm. The threshold level is represented in Figure 9 by the red dotted horizontal and acts as a lower limit of the BC-norm. It may be noted that the β- and BC-norms in the current study yield fairly similar magnitudes of the equivalent local strain measure.

5.2.1 Excluded experiments

A total of 6 experiments were excluded or considered as non-valid. The initial two CA tests (pipes 1 and 2) were part of a pre-testing phase. They were mainly intended to facilitate the initial set-up of the experimental procedure and get an initial estimate of the fatigue strength of the selected piping geometry. Pipes 1 and 2 were respectively subjected to approximately 94000 and more than 2 million cycles prior to failure. Pipe 1 did however present leakage in location B and pipe 2 failed under a clamp of the fixture, see Figure 10, presumably due to fretting fatigue. It motivated preemptive measures to improve the surface roughness under the clamps, which successfully prevented fretting fatigue in the VA tests.

Pipes 3, 5, 7 and 18, were subjected to a VAG spectrum load sequence with maximum strain amplitude of about 0.3, 0.3, 0.2 and 0.15%, respectively. The total number of applied cycles for these four experiments was approximately 1124000, 543000, 1161000 and more than 13 million cycles.

- Pipe 3 failed in location B due to increased friction in the experimental set-up, which was remediated for consecutive experiments.

- Pipe 5 failed consistently in A, but the data collection failed unfortunately at an early stage of the experiment and was therefore considered non-valid.

- Pipe 7 presented also a consistent final failure in A, but was considered non-valid due to an intermediate repair of the specimen, which required unmounting of the pipe and a consecutive restart of the experiment.

- Pipe 18 was subject to relatively significant loosening of the upper fixture, which induced temporarily reduced maximum strain amplitudes during the

test. The test was terminated prior to leakage or failure and thus considered a run-out.

As a result of the above irregularities, these four VA tests were thus not included in the projected analysis. The current test series did thus provide 13 valid data points for the analysis. It may be noted that the previous investigation for welded piping component in [4] also considered 13 data points from the VA piping and Gaussian spectra experiments. The number of valid data points was considered to be sufficient to avoid too large variance in the computed results.

Figure 10. Failure of pipe 2 below a clamp of the fixture due to fretting fatigue.

5.2.2 Parameter estimation

The model parameters for the smooth piping component were estimated using only the experimental data from the valid VAG load sequences reported in Table 4, i.e. 13 observations were used. The estimated parameters for both investigated fatigue life models are presented in Table 5. For the Basquin relation only two parameters were estimated, α and β, whereas the parameters in the Langer equation are A, B and C. The estimated standard deviation of the random error in the logarithmic fatigue life is denoted $\hat{\sigma}$. It is approximately equal to the coefficient of variation of the fatigue life. The corresponding results for the welded piping component are reported in Table 6, which is reproduced from [4].

Table 5. Estimated model parameters and standard deviation of the random error based on the VAG data for the non-welded piping component.
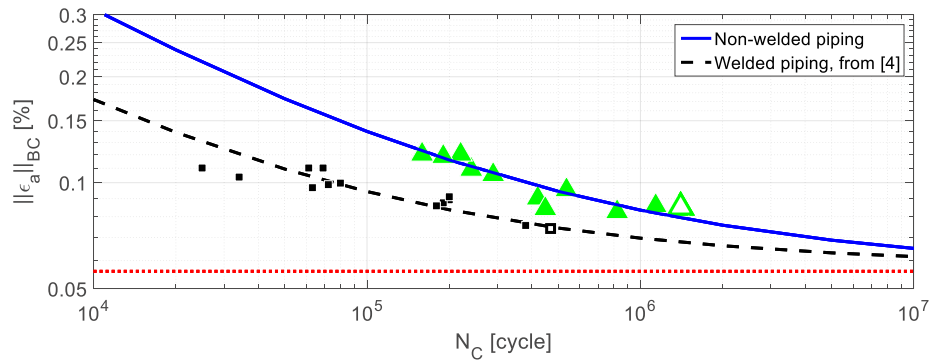
Model:	Factor		Slope		Cut-off limit		$\hat{\sigma}$
Basquin	$\hat{\alpha}$	141	$\hat{\beta}$	4.0	-		0.36
Langer	$\hat{A}$	591	$\hat{B}$	2.07	$\hat{C}$	0.056 %	0.36

Table 6. Estimated model parameters and standard deviation of the random error for the welded piping component in [4].

Model:	Factor		Slope		Cut-off limit		$\hat{\sigma}$
Basquin	$\hat{\alpha}$	2.89	$\hat{\beta}$	4.6	-		0.42
Langer	$\hat{A}$	128	$\hat{B}$	2.01	$\hat{C}$	0.058 %	0.36
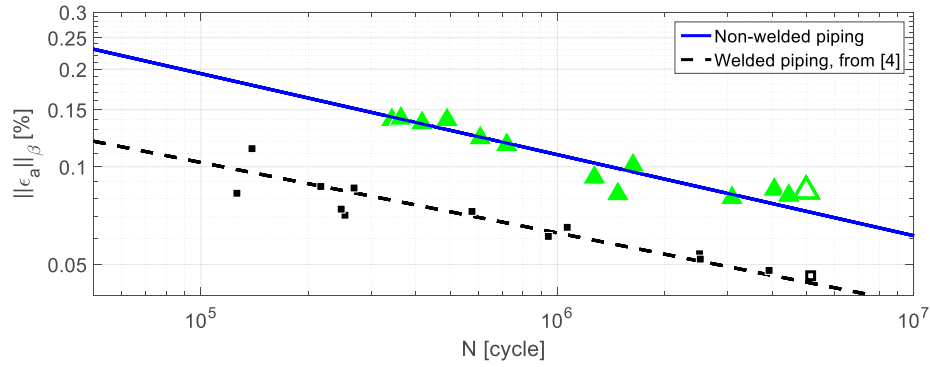
(a)

(b)

Figure 11. Estimated mean fatigue curves using the (a) Basquin fatigue model, and (b) Langer fatigue model with the red dotted horizontal representing C for the non-welded piping.

Figure 11 illustrates the obtained fittings for the non-welded or plain piping component with both considered fatigue models, see the blue solid curves and green triangular data points. The red dotted horizontal in Figure 11 (b) represents the value of the cut-off limit C obtained for the smooth non-welded piping component. The fitted mean curves and data points for the welded piping component studied in [4] are added for comparison in Figure 11, see the black dashed curves and square data points. Note however that the equivalent strain amplitudes for the welded component were computed based on the values for β, B and C reported in Table 6 or [4].

Comparison of Table 5 with the parameter estimates obtained for the welded piping component in Table 6 shows similar results for β, B and C. The difference in Basquin slopes for the welded and non-welded components can indeed be considered to be small, as illustrated graphically in Figure 11 (a). The 95% confidence interval (CI) of the difference in slope is estimated to (-1.02, 2.16), hence the difference is insignificant. However considerable differences for the factors α and A are observed, when comparing Table 5 and Table 6. The estimates for the non-welded component are indeed considerably larger than those obtained for the welded component. These factors directly relate to the vertical shift of the respective fatigue models, see Figure 11. Increased estimates of the factors α and A compared to the results related to the welded piping component is consistent with increased fatigue resistance for the smooth non-welded specimen.

The coefficients of variation of the estimated fatigue life in Table 5 are equal or smaller than those for the welded piping component in Table 6. A somewhat larger variation in fatigue life for a welded component may be related to a larger variation in defect sizes and material/weld quality for the welded piping component. The results in Table 5 indicate that both models yield identical standard deviation of the random error, thus none of the models shows better predictive capabilities. The difference between the two considered models is introduced by means of C. For the

current study, a 95% confidence interval for C was estimated to (0; 0.14%), thus including zero. Hence, C in the Langer model cannot be considered to be significantly different from zero. As mentioned previously, for $C=0$, the Langer model reduces to the Basquin model, thus both models can be expected to yield equivalent predictions.

5.2.3   Predicted number of load cycles causing fatigue damage

Contrary to the Basquin model, the Langer model assumes that only load cycles with strain amplitudes exceeding the cut-off limit C will contribute to causing fatigue damage. Hence, only a limited amount of load cycles applied to the testing component will define the actual fatigue life according to the Langer model. Figure 12 presents the ratio N_C/N for the Langer model, where N_C represents the number of strain cycles with strain amplitudes exceeding the limit C, and is also tabulated in Table 4. For the VAG spectrum, the amount of damaging load cycles included in the load sequences was ranging from 25 to 50% of the total number of load cycles. The ratio of damaging cycles decreases with increasing total number of cycles to failure, i.e. for decreasing load levels. For larger maximum strain amplitudes, more strain cycles are namely committed in the development of fatigue damage.
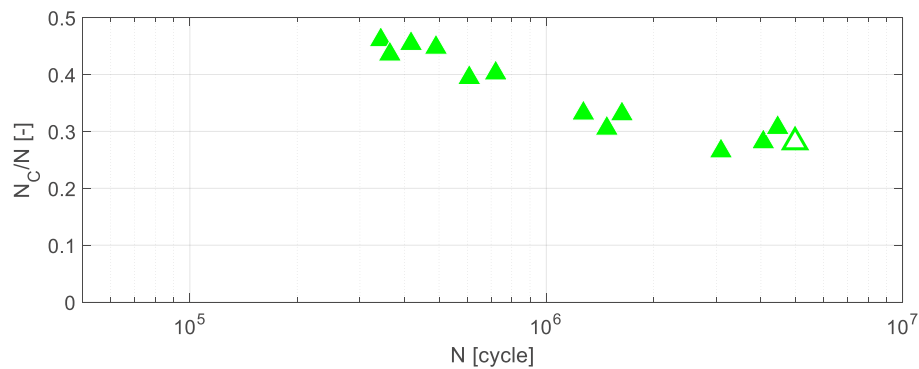

Figure 12. Predicted portion of number of load cycles contributing to fatigue damage based on the Langer model with C =0.056%.

5.3 Transferability

5.3.1 FSRF estimation

An apparent fatigue strength reduction factor for the welded piping component may be deduced graphically from Figure 11. Such an estimate does however omit the effect of different fatigue model parameters (β, B and C) in the equivalent strain amplitudes. A more consistent approach considers common parameter estimation using the data sets of both the welded and non-welded piping components. This approach was applied separately for both considered fatigue models, see results in Table 7. For the Langer model the cut-off limit C was fixed to 0.056%.

Table 7. Common estimated fatigue model parameters and corresponding estimated FSRF.

Model:	Factor		Slope		$\widehat{K}_f$ with 95% CI
Basquin	$\hat{\alpha}$	72.0	$\hat{\beta}$	4.41	1.89 (1.79;2.09)
Langer	$\hat{A}$	416	$\hat{B}$	2.22	1.79 (1.65;1.92)

It can be observed that the constant FSRF estimates in Table 7 do not differ significantly and have very similar confidence intervals. Figure 13 represents the common parameter estimation for the Langer model.
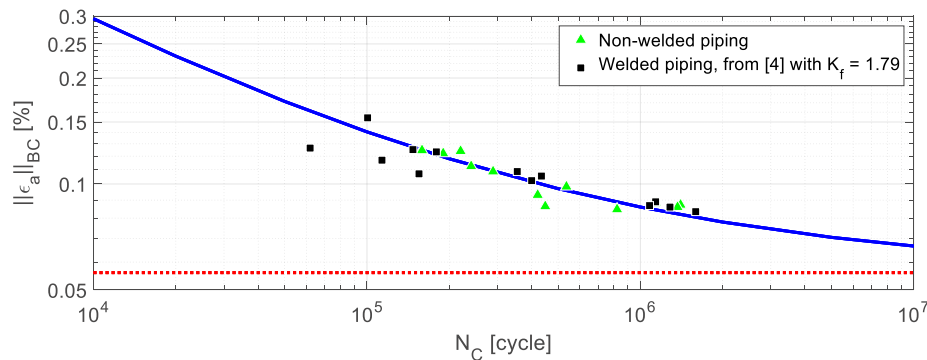

Figure 13. Langer fatigue model with common parameter estimation and with the red dotted horizontal representing the fixed cut-off limit of 0.056%.

### 5.3.2 Margins of ASME design curve

The 90% prediction limits for each fatigue model corresponding to 95% survival probability are interpreted as design curves specifically obtained from the performed experiments. These experimental design curves are compared to the ASME design curve. In the case of the welded piping component the ASME design curve is reduced similarly as in [4] but with the experimental estimate of the FSRF. The reduced ANL curve is then representing the mean curve for test specimens with a welding joint. For the smooth, non-welded specimens such reductions are not required.

5.3.2.1 Basquin model

The dashed lines in Figure 14 correspond to the mean curves, whereas the solid lines designate design curves corresponding to 95% survival probability. In particular, the red dashed line corresponds to the Basquin model fitted to experimental data represented by the square markers. The lower 90 % prediction limit for the Basquin model is computed from the estimated coefficient of variation of the fatigue life, and is represented by the red solid curve (Basquin design).
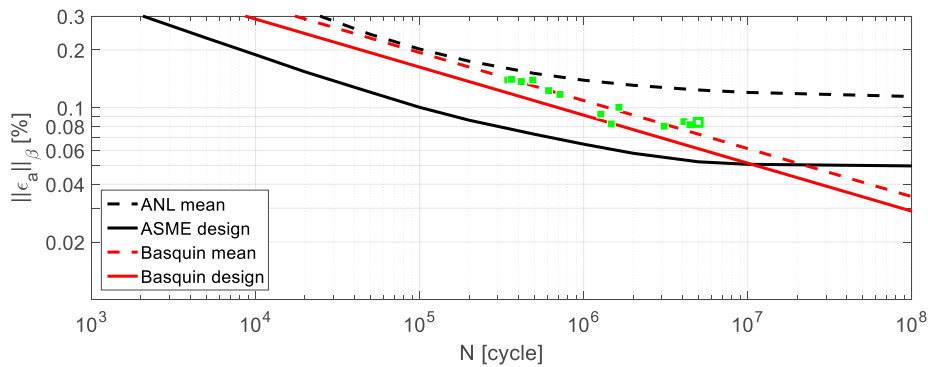
(a) Smooth, non-welded piping component with β-norm based on local strains.
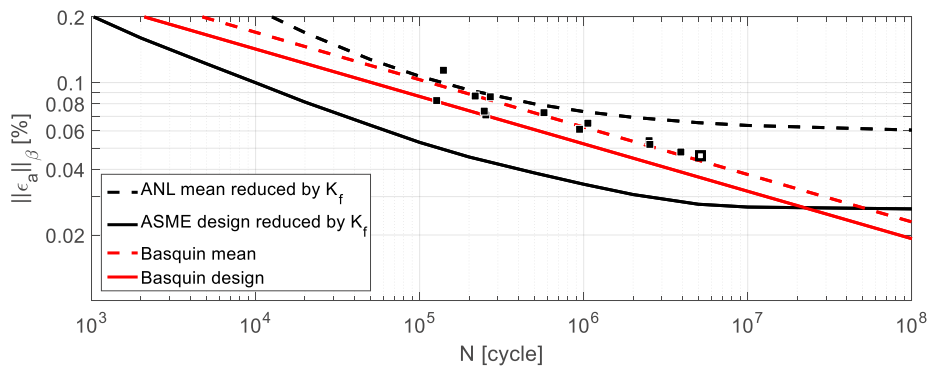
(b) Welded piping component, with K_f = 1.89 and β-norm based on nominal strains.

Figure 14. Comparison of the (reduced) ASME design curve and predictions using the Basquin model.
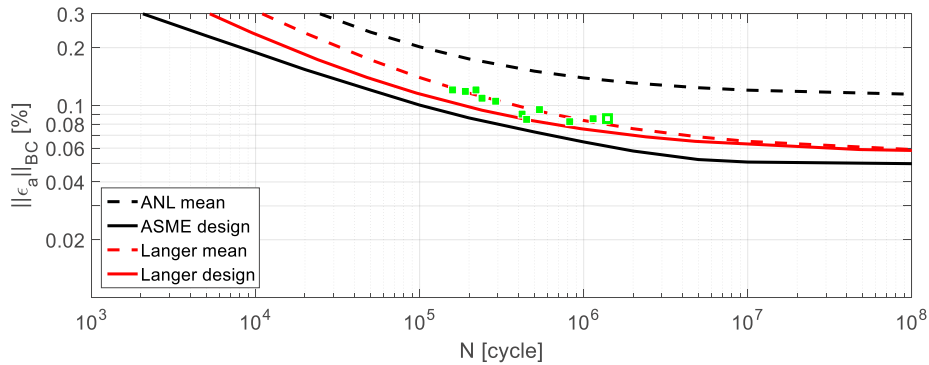
In Figure 14 (a), the black solid curve is the ASME design curve, as tabulated in [1], and the black dashed curve the ANL mean curve from [2]. These curves are directly relevant for the investigation of the smooth non-welded piping component considered in the current work. However, when considering the welded piping component from [4], a consistent reduction by K_f = 1.89, see Table 7, was performed. The resulting reduced ASME and ANL curves are shown in Figure 14 (b).

Figure 14 illustrates extensive conservatism in the ASME approach to transferability, as for the whole considered range of fatigue lives, the lower 90% prediction limit of the Basquin model is always situated above the relevant ASME design curve. ASME assumes the existence of a fatigue limit, whereas the Basquin equation has no fatigue limit, hence the comparison for extended fatigue lives is not relevant.
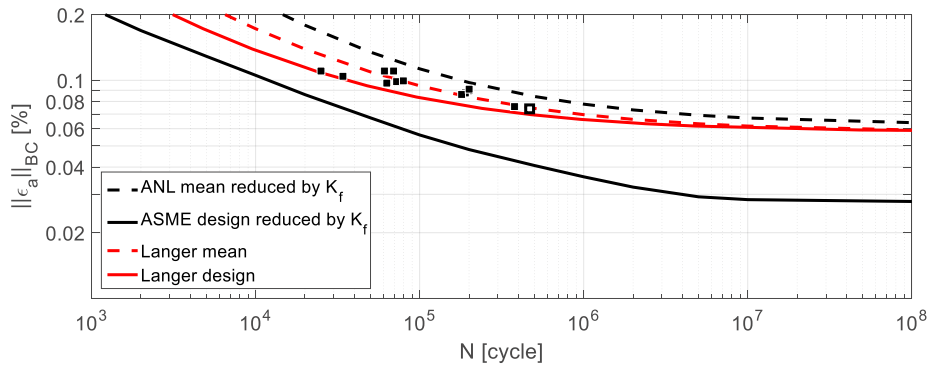
5.3.2.2 Langer model

The dashed lines in Figure 15 correspond to the mean curves, whereas the solid lines designate design curves corresponding to 95% survival probability. In particular, the red dashed line corresponds to the Langer model fitted to experimental data represented by the square markers. These experimental data points are plotted using the total number of cycles actually causing fatigue damage, i.e. N_C. The lower 90 % prediction limit for the Langer model is computed from the estimated coefficient of variation of the fatigue life, and is represented by the red solid curve (Langer design).

(a) Smooth, non-welded piping component with BC-norm based on local strains.

(b) Welded piping component, with K_f = 1.79 and BC-norm based on nominal strains.

Figure 15. Comparison of the (reduced) ASME design curve and predictions using the Langer model.

In Figure 15 (a), the black solid curve is the ASME design curve, as tabulated in [1], and the black dashed curve the ANL mean curve from [2]. These curves are directly relevant for the investigation of the smooth non-welded piping component considered in the current work. However, when considering the welded piping component from [4], a consistent reduction by K_f = 1.79, see Table 7, was performed. The resulting reduced ASME and ANL curves are shown in Figure 15 (b).

Figure 15 illustrates also the considerable conservatism in the ASME approach to transferability, as for the whole considered range of fatigue lives, the lower 90% prediction limit of the Langer model is always situated above the relevant ASME design curve. The use of the Langer model to investigate the margins in the ASME design curve is consistent, as the ANL curve from which the ASME design curve was derived, is also based on the Langer model. The fitted mean and lower 90% prediction limit are for both piping components situated in between the relevant ANL and ASME curves. Conservatism is preserved at HCF.

6 Discussion

The current investigation is a continuation of previous work on the margins in the fatigue design curve for austenitic stainless steel in ASME III [1]. The extent of the ASME margins was shown in [4] to largely depend on the value of the weld fatigue reduction factor used to reduce the original ASME design curve tabulated in [1]. The reduction was necessary to allow direct comparison with experimental results based on nominal strain recordings. The focus of the current investigation was an experimental estimate of a FSRF for the examined circumferential butt weld and a re-evaluation of the ASME margins.

In the current study, a series of fatigue tests on smooth piping components was performed under similar realistic testing conditions as in [4]. The experimental set-up and testing procedure were indeed identical, which is beneficial to a relevant and accurate FSRF estimation. The current investigation aimed at determining the fatigue strength for a straight un-notched smooth piping component, which was approximated with a piping geometry including a large circumferential notch in the center of the specimen. The selected geometry was motived by a reduction of test volume and allowed localization of fatigue failure. The tested notched piping component has however a lower fatigue strength than the un-notched piping component. This difference is expected to directly affect the FSRF estimation for the weld. However, the fatigue strength reduction due to the notch was assessed to be about 6%. The minor reduction in fatigue strength is mainly due to the relative notch insensitivity of austenitic stainless steel. Hence, the performed experiments were expected to provide a good approximation of the fatigue strength for an un-notched smooth piping component. It was also noted that the surface roughness on the inside of the smooth piping components was somewhat larger than in the previous study. Larger surface roughness is beneficial to fatigue initiation, but the predominant cyclic bending loads are expected to induce fatigue initiation in the machined notch on the outside surface of the specimens. The increased surface roughness on the inside will therefore not affect the results of the current investigation.

The material composition of the test specimens was also similar to the one in the previous investigation, but differences in the manufacturing process of the piping components existed. The current specimens were hot worked (extruded), whereas the pipes in [4] were initially cold worked (rolling). The latter specimens were however joined through welding, thus the original cold worked base material in the vicinity of the welding joint was subjected to additional heating. The effects of cold working will thus locally (in heat affected zone) be reversed by the subsequent welding procedure. Hence, the material in the vicinity of the welding joint is expected to be to some extent similar to the one of the hot worked pipes used in the current study. The effect of the initial difference in manufacturing process on the fatigue behavior is thus expected to be small. If any effects of the cold work were to remain for the material in the vicinity of the welding joint, it would primarily cause a reduction of the material's ductility for the welded piping component. As in [4], important inelastic material behavior was observed for the current non-welded specimens. A certain enhancement was even expected, due to recording of local axial strains in the notch. Furthermore was the use of annealed austenitic stainless steel favorable for the current study with notched specimens due to its low notch sensitivity.

Ratchetting or progressive accumulation of inelastic axial strain was recorded and could considerably affect the axial mean strain. The recorded increase in axial mean strain depended strongly on the severity of the cyclic load, as illustrated in Figure 6. The larger the cyclic loading, the larger the accumulation of inelastic strain. An increase in axial mean strain indicates permanent deformation and geometry change of the specimen. A certain elongation of the test specimen could be induced due to

the ratchetting in the axial direction. Curving of the piping could also occur due to a difference in axial elongation between locations A and B. The experimental set-up based on displacement control did however not adjust for such geometry changes. As a result some additional membrane or bending loads could be progressively introduced during testing. The change in mean axial strain never exceeded 1%. The expected geometry changes due to ratchetting were assumed to be relatively small, as assumed mainly localized in the notch of the specimen in the vicinity of locations A and B. It may also be noted that only specimens subjected to severe cyclic loading showed a considerable amount of ratchetting. The other experiments only presented a limited amount of accumulation of inelastic axial strain. Similar ratchetting is expected to have occurred in the welded piping experiments reported in [4]. Finally the occurrence of ratchetting in these realistic experiments highlights the inevitable occurrence of ratchetting in real-life applications in austenitic stainless steel subjected to cyclic loading.

Some differences in fatigue testing potentially affecting the estimate of the experimental FSRF were noted, but considered negligible. Hence a fatigue strength reduction factor for the circumferential butt weld was estimated to about 1.8, see Table 7. The Basquin and Langer models yielded very consistent estimates of the FSRF. It may be noted that the experimental estimate is considerably less than the general conservative ASME estimate which was 3.24. The ASME estimate is actually the product of two stress indices both equal to 1.8. The estimate based on a simplified numerical approach detailed in [4] yielded 1.4, which is considerably closer to the experimental result, but non-conservative. The non-conservatism is mainly due to geometric modelling assumptions of the weld toe in the performed FE analysis. The simplified numerical approach assumes that the computed notch factor is a conservative estimate of the FSRF. The reported numerical estimate was generated assuming an equivalent notch radius of 1 mm at the weld toe and an average element size of about 0.1 mm. The numerical approach to estimate the FSRF for the considered piping component can thus be improved by selecting a smaller equivalent notch radius and consequently a smaller element size near the weld toe. Indeed a smaller notch radius in an FE model will induce a larger notch factor.

The FSRF has been assumed to be constant and thus independent of the load level or number of cycles. With the Basquin model the 95% CI of the difference in slope for the non-welded and welded piping components included namely zero. Consequently the difference in slope is considered to be insignificant. Identical slopes effectively eliminates the load level dependence of the FSRF. A constant FSRF induces also good alignment of the data points with the Langer model, see Figure 13. No clear dependency from the load level or number of load cycles could thus be identified. The experimental results did thus not support the fatigue life dependency of the FSRF reported in [3]. This discrepancy may however be related to the considered range of load levels mainly focusing on the HCF regime and not really on LCF, where lower fatigue strength reduction factors may be observed [3].

The ASME margins could be re-evaluated for the welded piping component from [4] using the consistent experimental estimates of the FSRF derived in the current study. The evaluation is performed by comparison of the reduced ASME design curve and the empirical, component specific design curve derived in [4]. These curves both correspond to a 95% survival probability. The former is mainly based on CA data with smooth test specimens, whereas the latter was based on VA data for a realistic component. Considerable conservatism for the ASME design curve is highlighted in Figure 14 (b) and Figure 15 (b), thus irrespective of the used fatigue model. The use of the Langer model does however maintain consistency with the fitting of the ANL mean curve and consequently the resulting ASME design curve. For the welded piping component the ASME design curve is thus representing a survival probability largely in excess of 95%.

The experimental design curve in Figure 15 (b) can be translated to tangent the reduced ASME design curve, which allows to quantify a minimal margin. A horizontal translation of the experimental design curve corresponds to a reduction in number of cycles with a factor 2.3. The vertical translation corresponds to a reduction of the load level and equals at least 1.3. Both design curves tangent in the region below 104 cycles. Hence for HCF the margins are expected to be larger. The minimum margins for the smooth piping component are less than those for the studied welded piping. The horizontal and vertical translations of the experimental design curve for the smooth piping tangent the ASME design curve for reduction factors 1.6 and 1.14 respectively. Comparison between the mean curves in Figure 15 illustrates the need for a transferability correction to take amongst others differences in load and geometry into account.

The results presented in the current study highlight the over-conservatism of the ASME fatigue procedure to transferability for the considered piping components. This observation is consistent with a proposal to decrease the adjustment factor for the number of cycles from 12 to 10 in a preliminary revised version of the ANL report [2]. Such a modification would correspond to a horizontal (rightwards) shift of the ASME design curve with a factor 1.2. This factor is however less than the estimated minimal margins in fatigue life for the considered piping components. Conservatism of such a modified ASME design curve will thus be preserved for the considered components.

The ASME design curve is supposed to represent a 95% survival probability for a vast population of various piping components, loading conditions, etc. The presented results in the current study are however particular to the investigated components and their geometry. The fatigue life of the component was defined by leakage, which is directly affected by the wall-thickness of the component. Piping components with increased wall thicknesses are therefore expected to exhibit increased fatigue lives. Similarly pipes with increased diameter would be subjected to increased bending loads, resulting in higher load levels. Finally a welding joint and its properties will strongly affect the fatigue strength of the component.

The experimental design curves based on the Langer model practically coincide with the mean curves for large number of cycles, see Figure 15. This observation has already been made in the previous study [4]. It is due to the empirical approach using the estimated coefficient of variation of the fatigue life in the derivation of a design curve through a horizontal shift. Information on the variation of the fatigue limit would be valuable for an estimation of a vertical shift. Such a shift would greatly affect the experimental design curve in the HCF regime. Performing such an additional correction is consistent with the adjustment procedure behind the ASME design curve, where a factor of 2 on the load level was used [2].

The cut-off limit C in the Langer model introduces curvature and an asymptote in the SN curve. It should however only be interpreted as an estimate of a fatigue limit when a sufficient number of data points for large number of cycles are included. The extensive 95% confidence interval of the cut-off limit illustrates the large uncertainty about C, which cannot be considered to be significantly different from zero. It does thus not allow to show a clear difference in predictive capability of the two considered fatigue models.

7 Conclusions

In the current investigation fatigue tests on water pressurized non-welded austenitic stainless steel piping components were performed, with a realistic synthetic spectrum loading and particular focus on HCF. A weld fatigue strength reduction factor (FSRF) for a piping component with circumferential butt weld from [4] in as-welded condition was estimated. The resulting margins in the fatigue design curve for austenitic stainless steel in ASME III [1] were investigated. The obtained results and/or findings of the performed investigation are as follows:

- Inelastic material behavior was observed during fatigue testing, in particular for the higher load levels. A progressive increase in axial mean strain is due to ratchetting in the axial direction of the piping.

- Axial ratchetting is expected to have occurred also for the fatigue tests with the welded piping component.

- A conservative estimate of the FSRF for the considered welded piping component is about 1.8.

- The experimental estimate of the FSRF is significantly lower than an ASME estimate based on stress indices. Hence, significant conservatism of the ASME approach.

- The weld fatigue strength reduction does not exhibit any dependency on load level or number of load cycles.

- The Basquin and Langer fatigue models showed identical predictive capabilities for the non-welded piping component.

- The FSRF estimation using different fatigue models yielded consistent results.

- Extensive conservatism in the ASME approach to deal with transferability is confirmed for both welded and non-welded piping components.

- For the considered piping components the ASME design curve represents a survival probability largely in excess of 95 % for realistic load spectra.

- For the welded piping, the ASME design curve corresponds to a reduction in allowable number of cycles with a factor of at least 2.3. For the non-welded piping component the fatigue life reduction factor is minimum 1.6.

The experimental investigation resulted in increased understanding of the effect on the fatigue strength for piping components of a welding joint in as-welded condition. It improved the knowledge on the crucial issue of transferability and increased fundamental understanding for fatigue in piping components.

8 Recommendations

The performed investigation dealt with a specific piping geometry which was fatigue tested under specific loading conditions. The FSRF for a particular welding joint was determined. The limitations of the study can to some extent be resolved considering the following actions:

- The complex material behavior of austenitic stainless steel yielded locally relatively large inelastic deformations. It is therefore recommended to further investigate and verify whether the observed axial ratchetting behavior can be modelled based on the recommendations formulated in [18].

- The current and previous experimental investigations considered a fairly small and thin-walled piping component. Generalization of the findings to larger and thicker piping components relevant in nuclear applications can be verified by performing additional fatigue tests on piping components with for instance wall thicknesses in the range 6-12 mm.

- The experimentally derived FSRF is specific to a circumferential butt weld in as-welded condition. The effect on the fatigue strength of a piping component of other welding configurations or different welding process parameters is highly valuable for accurate fatigue life assessment of applications. To increase the understanding of these effects on the fatigue life of piping components, additional fatigue tests can be performed using the empirical procedure derived in the current investigations.

9 Acknowledgement

10 References

[1] ASME, "Boiler and Pressure Vessel Code, Section III, Rules for Construction of Nuclear Facility Components," 2013.

[2] O. Chopra and W. Shack, "Effect of LWR Coolant Environments on the Fatigue Life of Reactor Materials," NUREG/CR-6909, 2007.

[3] C. E. Jaske, "Fatigue-Strength-Reduction Factors for Welds in Pressure Vessels and Piping," *Journal of Pressure Vessel Technology,* vol. 122, pp. 297-304, 2000.

[4] M. Dahlberg, D. Hannes and T. Svensson, "Evaluation of fatigue in austenitic stainless steel pipe components," SSM 2015:38, 2015.

[5] T. Svensson, D. Hannes, P. Johannesson, M. Dahlberg and A. Anderson, "Three HCF models for strain fatigue life of welded pipes in austenitic stainless steel," *Procedia Engineering,* vol. 101, pp. 476-484, 2015.

[6] M. Dahlberg, D. Hannes and Z. Chen, "Fatigue fracture surface characterization and investigation," SSM 2016:28, 2016.

[7] M. Dahlberg and D. Hannes, "Validation of fatigue fracture mechanics approaches," SSM 2016:27, 2016.

[8] A. Palmgren, "Die Lebensdauer von Kullagern," *Zeitschrift des Vereins Deutscher Ingenieure,* pp. 339-341, 1925.

[9] M. Miner, "Cumulative damage in fatigue," *J. Appl. Mech.,* vol. 12, pp. 159-164, 1945.

[10] P. Johannesson, T. Svensson and J. de Maré, "Fatigue life prediction based on variable amplitude tests," *Int. J. Fatigue,* vol. 27, pp. 954-965, 2005.

[11] O. Basquin, "The exponential law of endurance tests," *Proc. ASTM,* vol. 10, pp. 625-630, 1910.

[12] B. Langer, "Design of Pressure Vessels for Low-Cycle Fatigue," *ASME J. Basic Eng.,* vol. 84, pp. 389-402, 1962.

[13] Y. Weixing, X. Kaiquan and G. Yi, "On the fatigue notch factor, Kf," *International Journal of Fatigue,* vol. 17, no. 4, pp. 245-251, 1995.

[14] S. D. Sheppard, "Field Effects in Fatigue Crack Initiation: Long Life Fatigue Strength," *Journal of Mechanical Design,* vol. 113, pp. 188-194, 1991.

[15] C. Yen and T. Dolan, "A Critical Review of the Criteria for Notch-Sensitivity in Fatigue of Metals," University of Illinois, Urbana Champaign, 1952.

[16] B. Sundström, Handbook of Solid Mechanics, Stockholm: Department of Solid Mechanics KTH, 2010.

[17] J. Colin and A. Fatemi, "Variable amplitude cyclic deformation and fatigue behaviour of stainless steel 304L including step, periodic, and random loadings," *Fat. Fract. Eng. Mat. Struct.,* vol. 33, pp. 205-220, 2010.

[18] M. Möller, A. Gustafsson and P. Segle, "Robust structural verification of pressurized nuclear components subjected to ratcheting," SSM 2015:43, 2015.

2017:25

The Swedish Radiation Safety Authority has a comprehensive responsibility to ensure that society is safe from the effects of radiation. The Authority works to achieve radiation safety in a number of areas: nuclear power, medical care as well as commercial products and services. The Authority also works to achieve protection from natural radiation and to increase the level of radiation safety internationally.

The Swedish Radiation Safety Authority works proactively and preventively to protect people and the environment from the harmful effects of radiation, now and in the future. The Authority issues regulations and supervises compliance, while also supporting research, providing training and information, and issuing advice. Often, activities involving radiation require licences issued by the Authority. The Swedish Radiation Safety Authority maintains emergency preparedness around the clock with the aim of limiting the aftermath of radiation accidents and the unintentional spreading of radioactive substances. The Authority participates in international co-operation in order to promote radiation safety and finances projects aiming to raise the level of radiation safety in certain Eastern European countries.

The Authority reports to the Ministry of the Environment and has around 300 employees with competencies in the fields of engineering, natural and behavioural sciences, law, economics and communications. We have received quality, environmental and working environment certification.